Supporting Information

Probing Protein Dynamics using Multi-Field Variable Temperature NMR Relaxation and MD Simulation

Baptiste Busi,[1] Jayasubba Reddy Yarava,[1] Albert Hofstetter,[1] Nicola Salvi,[2] Diane Cala-De Paepe,[3] Józef R. Lewandowski,[4] Martin Blackledge, [2] and Lyndon Emsley*[1]*

[1] Institut des Sciences et Ingènierie Chimiques, Ecole Polytechnique Fédérale de Lausanne (EPFL), 1015 Lausanne (Switzerland)

[2] Univ. Grenoble Alpes, CNRS, CEA, IBS, 38000 Grenoble, France.

[3] Université de Lyon, Institut des Sciences Analytiques (UMR 5280 CNRS/UCBL/ENS Lyon), Centre de RMN à Très Hauts Champs, 69199 Villeurbanne (France)

[4] Department of Chemistry, University of Warwick, Coventry CV4 7AL, United Kingdom

E-mail: martin.blackledge@ibs.fr and lyndon.emsley@epfl.ch

Table of Contents

Sample Preparation **3**

Experimental **3**

Experimental and Computational Details **4**

Pulse sequences *4*

Relaxation Rate Equations *5*

Experimental Data **6**

Spectra *7*

Signal Intensities *7*

Relaxation Rates and Motional Models **7**

Relaxation Rates with Single Field and Simultaneous Fits *7*

Numerical Values of Fit Parameters *7*

Cross-Validation **10**

MD simulation **11**

Sample Preparation

The Uniformly ^{13}C,^{15}N labelled GB1 protein was purchased from Cortectnet. First the buffer was replaced by extensive dialysis against 50 mM sodium Phosphate buffer (pH 5.5). The protein was concentrated to 25 mg.ml^{-1}. A mixture of 1:2 isopropanol:methyl-2-4-pentane-diol was used for precipitation of the protein by adding 3 volumes of the mixture for 1 volume of protein solution which give the sample the appearance of a milky solution. [1] The obtained microcrystals are then introduced in the 3.2 mm rotor by ultracentrifugation using Giotto Biotech device (100 000 g, 4°C) in order to sediment most of the microcrystals and remove as much as possible of the supernatant. [2] The rotor is stored at 4°C between experiment sessions.

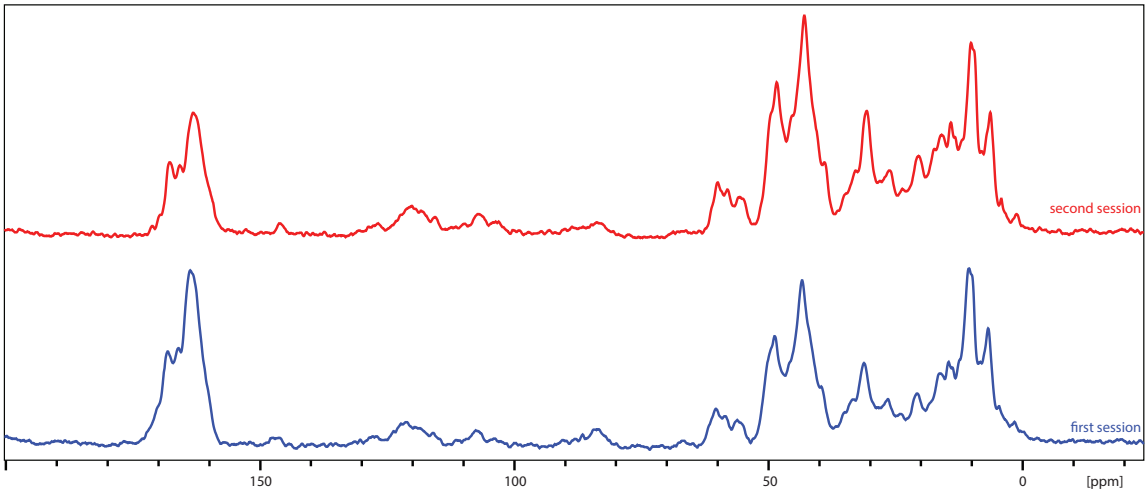

Figure S1: Comparison of ^{13}C NMR spectra from one session to another. (277.4 K, 11.75 T)

Experimental

Solid state NMR measurements were carried out on Bruker AV-I 9.4 T, AV-IIIHD 11.75 T, AV-III 14.1 T and AV-III 18.8 T spectrometers. For all the measurements 3.2 mm low temperature MAS probes were used in triple resonance (^{1}H,^{13}C,^{15}N) mode. 6 different relaxation parameters (R_1) were extracted by using different experimental methods. They are ^{1}H ($R_{1,direct}$, $R_{1,CP}$), $^{13}C_{methyl}$, $^{13}C'$, ^{15}N backbone and ^{15}N in the lysine sidechain. 10 kHz magic angle spinning (MAS) was used for all the measurements.

The measurements were performed on two batches of GB1 protein. The 11.75 T data was extracted on the first batch of GB1, and 9.4 T, 14.1 T, 18.8 T measurements were done on a second batch of GB1. Each of these 6 measurements was made as a function of the temperature, going from 105 K to 285 K in steps of 5 or 10 K. VT, Bearing and Drive display temperatures were held identical in the cooling cabinet, in order to minimise temperature gradients across the sample. All the noted temperatures had a precision of +/- 10 K. At 11.75 T, measurements were carried out twice, first with an increasing order of temperatures and a second time with a random order of temperatures.

Experimental and Computational Details

Pulse sequences

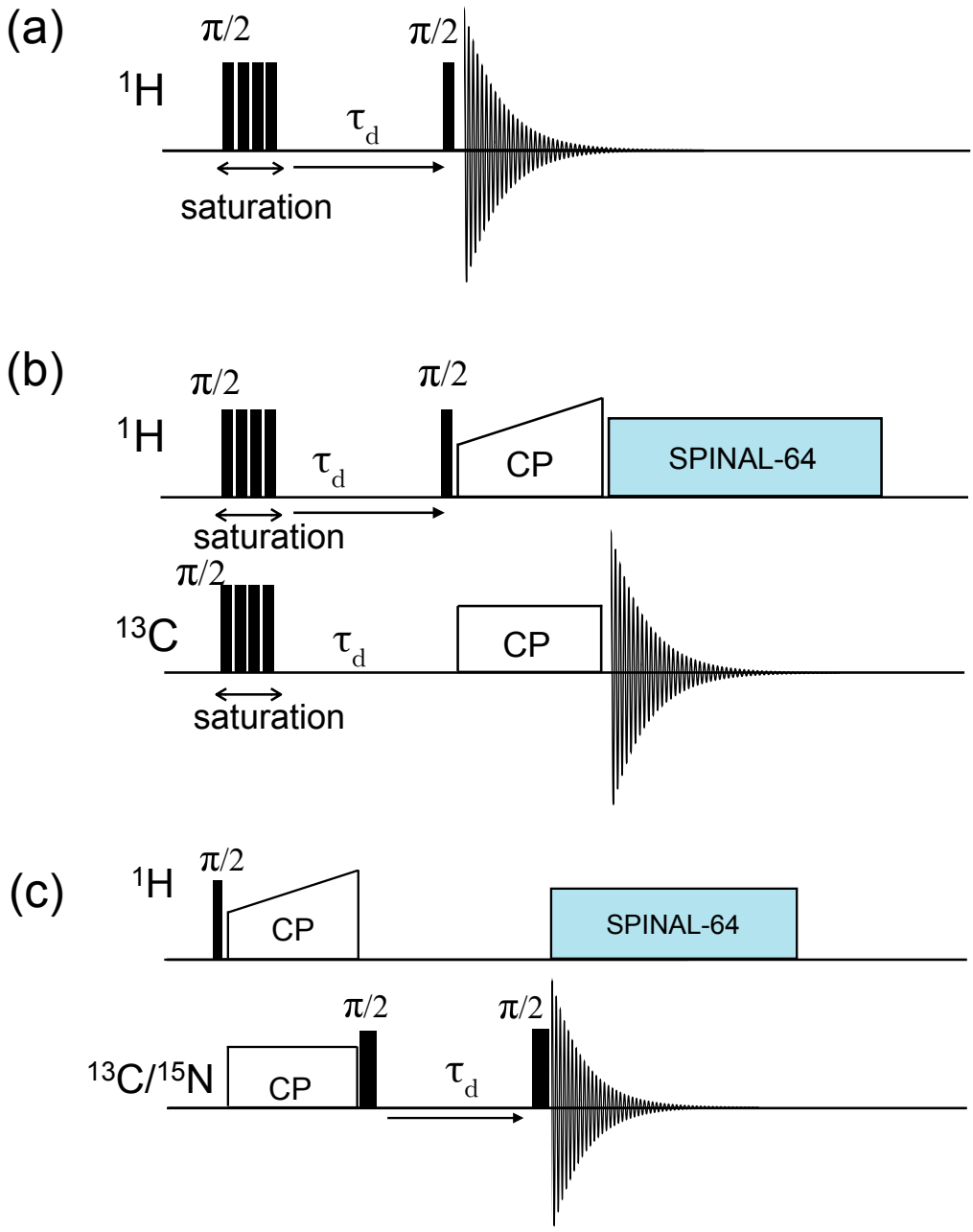

Figure S2: Schematic representation of the pulse sequences. a) R_1 measurement for ^1H b) ^{13}C detected R_1 measurement for ^1H c) R_1 measurement for heteroatoms (^{13}C, ^{15}N).

Relaxation Rate Equations

NMR relaxation is mainly caused by fluctuations of the anisotropic interactions, like the CSA tensor or the dipolar couplings due to rotational motions of the nuclei. Thus the relaxation rates of individual transitions can be used to report on different regions of the protein. Here we use ^{13}C relaxation from the backbone C' or from the methyl group, ^{1}H relaxation from the hydration shell or bulk solvent, and ^{15}N relaxation from the backbone or the lysine side chain. The different spy nuclei can be selected by using different pulse sequences or the difference in the respective chemical shifts of the nuclei (see figure S2). At low temperatures resolution in the NMR spectrum degrades[3-6] such that site-specific information is no longer accessible, but type specific information is still resolvable. Thus, the rates we measure here are the sum of the contributions from all of the nuclei of a given type in the protein. We measure the relaxation parameters T_1. Fast motion (ps-ns) will be efficient in inducing spin-lattice relaxation (T_1), while slower motion (ns-ms) will have more impact on the relaxation in the rotating frame ($T_{1\rho}$) or on spin-spin relaxation (T_2').[7]

For ^{13}C and ^{15}N we determined the reported relaxation rates by fitting the initial slope of the data to a single exponential Ae^{-t/T_1} , with A and T_1 as fitting parameters. The ^{1}H measurements were acquired using saturation recovery experiments. Thus, we fitted the curves to $A(1 - e^{-\frac{t}{T_1}})$ with A and T_1 as fitting parameters.

Here we use Redfield theory to describe relaxation.[8] We assume that each motional mode has a temperature dependent rate of motion according to an Arrhenius relation[9] as follows

$$\tau_k = \tau_{\infty,k} e^{(E_k/RT)} \quad (1)$$

Where τ_k is the correlation time of motion at a given temperature (T) and E_k denotes the activation energy for the mode. The correlation times are related to the relaxation times through the spectral densities presented below.

The following expressions have been assumed for the different relaxation rates.[10]

spin-lattice relaxation for proton

$$R_1 = C_{interaction}(J(\omega_H) + 4J(2\omega_H))$$

dipolar spin-lattice relaxation for heteroatoms

$$R_1^{DD} = C_{interaction}(J(\omega_H - \omega_X) + 3J(\omega_X) + 6J(\omega_H + \omega_X))$$

CSA spin-lattice relaxation for heteroatoms (not for methyl R_1 because the CSA is negligible compared to other relaxation processes)

$$R_1^{CSA} = C_{interaction} J(\omega_X)$$

We assume a Gaussian-Markoff process for the individual motional modes. This results in a spectral density $J(\omega)$ at frequency ω, represented as a sum of the different modes.

$$J(\omega) = \sum_{k=1}^{N} C_{k,amplitude} \frac{\tau_k}{1 + \omega^2 \tau_k^2}$$

where $J(\omega)$ denotes the spectral density at a given frequency ω, with N being the number of different motional modes (in our case from 1 to 3). $C_{k,amplitude}$, is a dimensionless factor associated with the amplitude of the motion,

which can also be described through the order parameter of the motion. Note that in the following we assume that the amplitude of motion is constant as a function of temperature. This simplification is necessary to avoid overfitting the relaxation data. ω_H is the proton Larmor frequency, ω_X the the heteroatom Larmor frequency (^{13}C or ^{15}N) and ω_1 the nutation frequency of the rf field.

C_k is the product of factor associated with the amplitude, and the interaction of the motion ($C_k = C_{k,amplitude} \times C_{interaction}$).

When possible, $C_{interaction}$ was explicitly expressed.

The $C_{interaction}$'s are given as,

^{15}N dipolar R_1

$$\frac{1}{10}\left(\frac{\mu_0\gamma_H\gamma_N\hbar}{4\pi r_{NH}^3}\right)^2$$

^{15}N CSA R_1

$$\frac{2}{15}\omega_N^2(\sigma_\parallel - \sigma_\perp)^2$$

^{13}C dipolar R_1 C'

$$\frac{1}{10}\left(\frac{\mu_0\gamma_H\gamma_C\hbar}{4\pi r_{CH}^3}\right)^2$$

^{13}C dipolar R_1 methyl

$$\frac{3}{10}\left(\frac{\mu_0\gamma_H\gamma_C\hbar}{4\pi r_{CH}^3}\right)^2$$

^{13}C CSA R_1 C'

$$\frac{2}{15}\omega_C^2(\sigma_\parallel - \sigma_\perp)^2$$

γ_X represent the gyromagnetic ratio of the X atom, μ_0 denotes the permeability of free space, $\hbar$ the plank constant$\sigma_\parallel - \sigma_\perp$ the chemical shift tensor (assumed axially symmetric for a first approximation) with the value of -160 ppm for the N-H coupling in the amide bond, -15 ppm for the N-H coupling of the lysine side chain, -172 ppm for the carbonyl-proton coupling of the carbonyl and negligible for the methyl.

r_{CH} respectively r_{NH} denote the average inter-nuclear distance between the two atoms, given as 1.115 Å for the C-H coupling of the methyl, 2.04 Å for the C-H coupling of the carbonyl and 1.02 Å for the N-H coupling.

Experimental Data

For R_1 relaxation measurements on ^{13}C and ^{15}N nuclei, a z-filter was incorporated after the CP step and during acquisition Spinal-64 decoupling was used. A saturation recovery experiment was used for ^{1}H direct R_1 and a CP block was used after the saturation recovery for ^{1}H R_1, CP measurements. For the 11.75 T data, 8 transients were used for all the measurements. For all other fields, 16 transients were used. The difference in number of transients for 11.75 T compared to other fields is due to a smaller sample quantity. For all experiments, a 3.2 mm zirconia rotor was used with vespel cap. Measurements were done for 19 (or 21) different temperatures. All the data, for each spectrometer, were obtained in one session except for the data at 18.8 T which was obtained during two different sessions. The sample was stored between the two sessions in the 3.2 mm NMR rotor in a fridge at 4 °C.

Spectra

The spectra are given in TopSpin format in a zip-file, *fullspectra.zip*.

Signal Intensities

The extracted signal intensities for all relaxation rates as a function of relaxation time, temperature and magnetic field strength are given in the excel files contained in the zip-file, *Signal_Intensities.zip*.

Relaxation Rates and Motional Models

Relaxation Rates with Single Field and Simultaneous Fits

The plots of the measured relaxation rates with the corresponding single field fits (400 MHz, 500 MHz (set **II**), 500 MHz (set **III**), 600 MHz and 800 MHz) and with the fits to the motional models are given below.

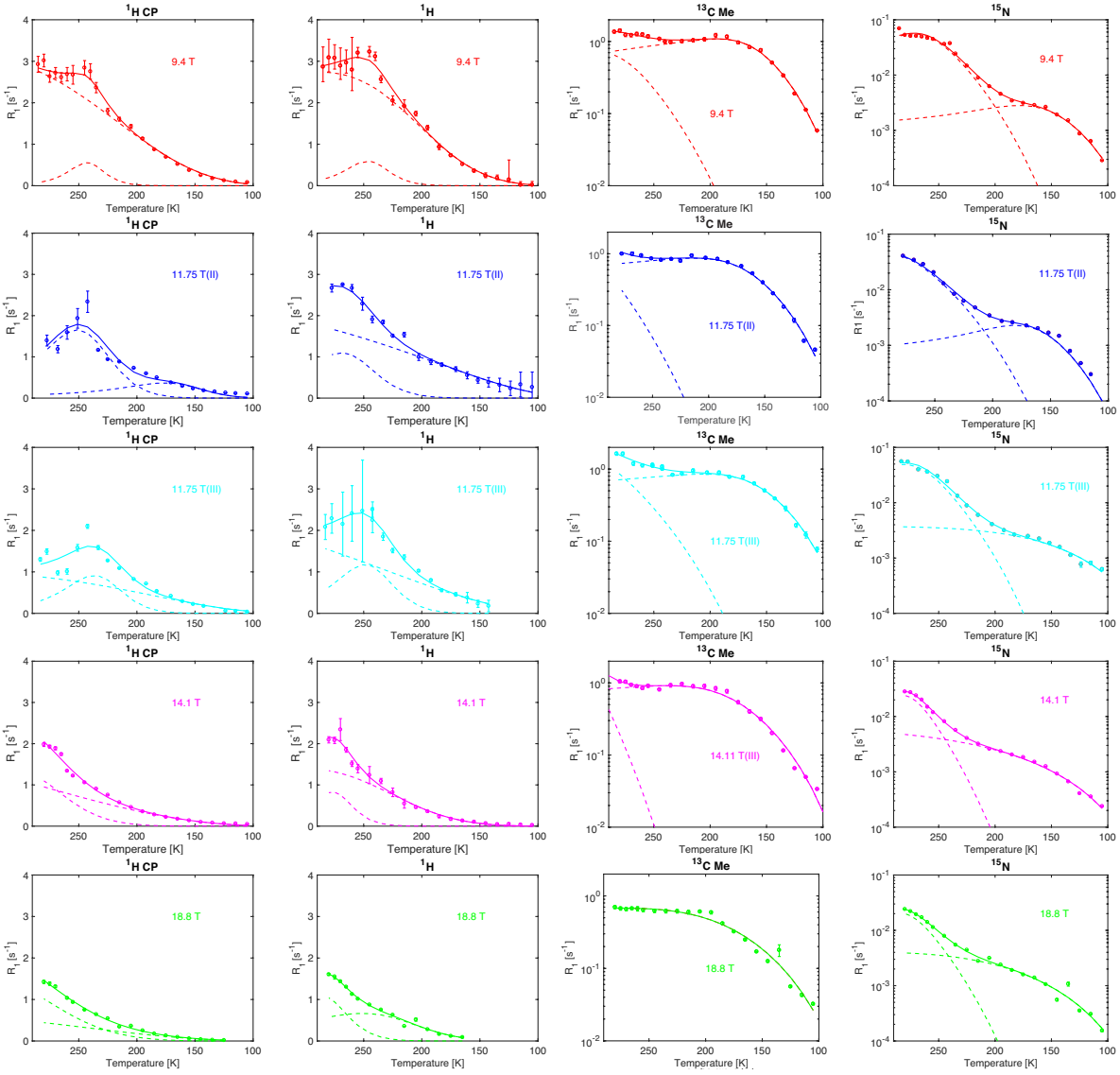

Figure S3: Single field fit of R_1 as a function of temperature. The number of modes is statistically justified by a F-test. ($P<0.05$).

Numerical Values of Fit Parameters

The numerical values for the fit parameters (E_k, τ_k, $C_{k,amplitude}$) of the different motional modes and their standard deviations, calculated with Monte Carlo standard deviations estimations over 500 runs, are given below.

Mode	Activation Energy (J/mol)	400 MHz	500 MHz set III	500MHz set II	600MHz	800MHz	Simultaneous fit	Sd	400 MHz	500 MHz set III	500 MHz set II	600 MHz	800 MHz	Simultaneous fit
1	^{1}HCP E 1	6.2E+03	4.2E+03	8.5E+03	8.1E+03	5.9E+03	4.6E+03		5.0E+02	1.3E+03	3.4E+03	1.5E+03	1.4E+03	4.7E+02
	^{1}Hdirect E 1	7.8E+03	4.8E+03	3.6E+03	9.5E+03	1.2E+04	5.6E+03		1.5E+03	1.3E+03	1.1E+03	2.2E+03	1.5E+03	5.0E+03
	^{13}Cmet E 1	7.3E+03	6.0E+03	6.9E+03	7.0E+03	5.7E+03	6.5E+03		1.9E+02	2.0E+03	1.5E+02	2.0E+02	2.0E+02	1.7E+02
	^{15}N R1 E 1	6.2E+03	3.4E+03	8.1E+03	4.5E+03	5.1E+03	6.4E+03		1.5E+03	7.2E+02	3.9E+02	1.5E+02	1.2E+02	6.1E+02
	^{15}N Lys E 1	4.4E+03	5.0E+03	3.2E+01	9.5E+03	5.4E+02	4.8E+03		2.8E+03	2.9E+04	1.9E+03	3.0E+03	1.1E+03	3.0E+02
2	^{1}HCP E 2	3.8E+04	2.2E+04	2.1E+04	1.8E+04	1.5E+04	3.2E+04		8.5E+03	4.4E+03	1.0E+04	4.2E+03	3.7E+03	1.9E+03
	^{1}Hdirect E 2	3.2E+04	2.4E+04	2.4E+04	4.4E+04	3.6E+04	1.9E+04		1.1E+04	6.2E+03	7.3E+03	1.1E+04	1.4E+04	1.2E+04
	^{13}Cmet E 2	2.4E+04	2.2E+04	3.2E+04	5.6E+04	3.4E+05	2.9E+04		4.7E+03	5.3E+03	1.1E+04	1.5E+04	3.7E+04	9.6E+03
	^{15}N R1 E 2	2.4E+04	2.7E+04	2.3E+04	3.8E+04	3.2E+04	2.2E+04		5.0E+03	3.8E+03	3.7E+03	3.3E+03	2.6E+03	3.0E+03
	^{15}N Lys E 2	6.0E+04	3.4E+04	2.5E+04	4.7E+04	4.1E+04	2.9E+04		7.9E+03	4.0E+03	7.1E+03	4.1E+03	4.1E+03	1.5E+02
3	^{1}HCP E 3	0.0E+00	0.0E+00	0.0E+00	3.3E+04	0.0E+00	3.3E+04		0.0E+00	0.0E+00	0.0E+00	5.4E+03	0.0E+00	9.9E+04
Mode	Correlation Time (s)	400 MHz	500 MHz set III	500 MHz set II	600 MHz	800 MHz	Simultaneous fit	Sd	400 MHz	500 MHz set III	500 MHz set II	600 MHz	800 MHz	Simultaneous fit
1	^{1}HCP τ 1	3.6E-11	5.9E-11	5.7E-13	4.9E-13	3.5E-11	1.8E-10		6.1E-10	2.5E-09	3.1E-09	7.7E-12	9.3E-11	3.1E-10
	^{1}Hdirect τ 1	9.4E-12	1.1E-10	1.5E-10	3.8E-12	4.3E-13	2.9E-11		1.8E-09	1.1E-09	1.2E-08	1.4E-09	1.5E-09	5.1E-09
	^{13}Cmet τ 1	1.3E-11	3.0E-11	2.1E-11	2.4E-11	5.2E-11	2.5E-11		2.5E-12	8.3E-12	3.0E-12	4.8E-12	1.1E-11	4.6E-12
	^{15}N τ 1	5.7E-11	8.5E-10	1.3E-11	8.2E-10	2.8E-10	3.8E-11		4.0E-10	3.8E-08	2.0E-08	1.1E-08	9.1E-10	1.7E-10
	^{15}NLys τ 1	2.1E-10	9.5E-11	1.6E-10	1.5E-12	2.6E-11	5.4E-11		2.0E-08	2.1E-10	2.4E-08	1.0E-10	5.0E-11	6.6E-11
2	^{1}HCP τ 2	1.7E-18	2.0E-15	9.4E-15	1.2E-14	6.6E-13	3.9E-17		1.5E-14	5.1E-14	1.5E-14	1.1E-13	1.9E-12	7.4E-18
	^{1}Hdirect τ 2	4.3E-17	1.5E-15	4.5E-15	8.8E-19	3.6E-17	2.7E-14		3.5E-14	8.3E-14	3.5E-14	1.9E-14	2.3E-17	9.0E-14
	^{13}Cmet τ 2	8.2E-14	6.2E-13	6.2E-14	4.0E-17	8.1E-12	2.5E-12		2.9E-12	6.6E-12	3.4E-12	4.0E-12	3.7E-12	5.3E-11
	^{15}N τ 2	1.1E-13	3.2E-14	2.4E-13	2.2E-16	2.4E-15	5.0E-13		6.1E-12	2.4E-13	2.0E-11	3.8E-14	1.9E-14	1.2E-11
	^{15}NLys τ 2	1.0E-22	2.6E-16	3.4E-15	2.5E-19	3.0E-18	4.5E-15		1.6E-18	2.6E-14	3.8E-13	2.3E-14	1.9E-14	2.6E-15
3	^{1}HCP τ 3	0.0E+00	0.0E+00	0.0E+00	1.5E-16	0.0E+00	4.4E-16		0.0E+00	0.0E+00	0.0E+00	1.2E-15	0.0E+00	2.1E-15
Mode	C	400 MHz	500 MHz set III	500 MHz set II	600 MHz	800 MHz	Simultaneous fit	Sd	400 MHz	500 MHz set III	500 MHz set II	600 MHz	800 MHz	Simultaneous fit
1	^{1}HCP Ck 1	5.9E+09	2.9E+09	8.1E+08	4.0E+08	2.7E+09	9.0E+09		3.9E+10	1.2E+11	6.7E+10	7.6E+08	6.8E+09	1.2E+10
	^{1}Hdirect Ck 1	4.8E+09	6.9E+09	6.8E+09	3.7E+09	2.3E+09	3.3E+09		1.9E+11	8.4E+10	2.8E+11	5.6E+11	1.5E+12	1.8E+11
	^{13}Cmet Ck 1	6.5E-02	3.1E-01	6.5E-02	8.2E-02	8.2E-02	7.0E-02		2.0E-03	5.7E-02	2.3E-03	5.6E-03	3.6E-03	3.5E-03
	^{15}N Ck 1	7.7E-04	1.2E-03	7.3E-04	2.3E-03	1.6E-03	6.8E-04		3.6E-01	4.0E-02	2.9E-01	2.8E-02	4.2E-03	7.0E-04
	^{15}NLys Ck 1	9.3E-04	1.4E-03	3.5E-03	1.1E-03	4.8E-03	7.4E-04		3.4E-02	1.7E-03	9.0E-03	3.2E-03	3.4E-03	2.1E-04
2	^{1}HCP Ck 2	9.9E+08	2.4E+09	3.7E+09	1.6E+09	5.7E+09	1.7E+09		5.0E+09	8.8E+08	3.6E+10	1.2E+09	1.4E+10	2.4E+08
	^{1}Hdirect Ck 2	1.1E+09	2.6E+09	2.4E+09	2.2E+09	3.8E+09	2.6E+09		2.0E+10	9.0E+08	9.7E+08	9.7E+10	2.1E+11	1.4E+11
	^{13}Cmet Ck 2	4.3E-02	9.2E-01	6.3E-01	8.3E+00	2.0E-01	7.0E+00		1.7E-01	1.8E-01	8.4E+01	8.4E+01	1.8E-01	1.5E+02
	^{15}N Ck 2	1.5E-02	1.6E-02	1.5E-02	8.7E-03	8.4E-03	1.6E-02		2.3E-03	2.9E-03	2.6E+01	1.1E-01	1.9E-02	1.3E-01
	^{15}NLys Ck 2	3.4E+01	1.5E+00	8.2E-03	1.8E+00	1.8E+00	1.1E+00		1.9E+01	4.3E-01	3.2E+00	1.9E-01	2.2E-01	1.2E-01
3	^{1}HCP Ck 3	0.0E+00	0.0E+00	0.0E+00	4.7E+09	0.0E+00	1.0E+09		0.0E+00	0.0E+00	0.0E+00	1.4E+10	0.0E+00	2.5E+09

Table S1: Numerical values for the fits of the relaxation parameters. The activation energy and the correlation time refer to the Arrhenius fit, and the C represent the $C_{k,amplitude}$ used in fit as described above. Sd stand for one standard deviation as a measure of error.

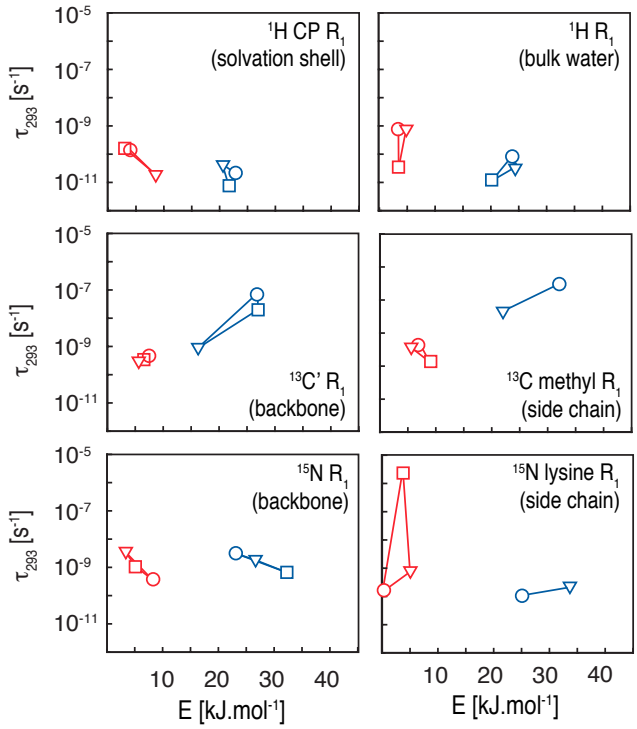

*Figure S4: Fitting of repeat measurements of each of the different relaxation rates (of which ^{15}N R_1 is shown in figure 1). For each mode presented, the fitted activation energy is plotted against the correlation time at 293 K, from $\tau_k = \tau_{\infty,k} e^{(E_k/RT)}$, for the three independent measurements. In each panel the red symbols show the low energy motional mode and the blue symbols show the higher energy mode. Squares show data set **I**, triangle show data set **II**, and circles show data set **III**. The lines connecting the symbols are intended as a guide to the eye, connecting the three data sets.*

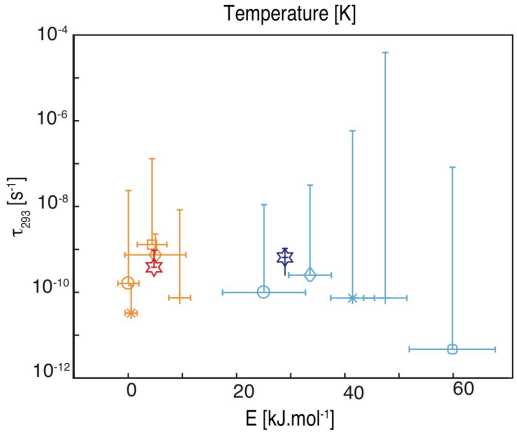

*Figure S5: The activation energies and correlation times at 293K, $\tau_k = \tau_{\infty,k} e^{(E_k/RT)}$, for $^{15}N_{Lys}$ extracted from the data in Figure 2 a). The red and blue symbols refer to the low energy and the high energy mode respectively for 9.4 T (square), 11.75 T (set **II**) (diamond), 11.75 T (set **III**) (circle), 14.1 T (cross), and 18.8 T (asterisk), and denote the values extracted from the single field fits. The bold stars show the values extracted from the simultaneous fit to all the data. The error bars are set to +/- one standard deviation, calculated with a Monte Carlo error estimation over 500 runs. Because of the logarithmic scales negative error bars are not displayed.*

Cross-Validation

For the cross-validation procedure (10-fold-split) the experimental data from the three sets (**I**, **II** and **III**) was combined and 90% of the combined data (R_1) was randomly sampled (training set) and used to predict the remaining 10% (validation set) of the experimental data (R_1). This procedure was repeated 100 times. The random sampling was restricted to avoid double sampling and to contain at least two data points per temperature range (±5 K). For ^{15}N lysine we only used the data sets **II** and **III** in the cross-validation procedure. Also for ^{15}N lysine only set **III** contains R_1 values above 220 K. Thus, the random sampling was only restricted to avoid double sampling. Figure S4 plots the experimental against the predicted R_1 values for both the training and the validation sets.

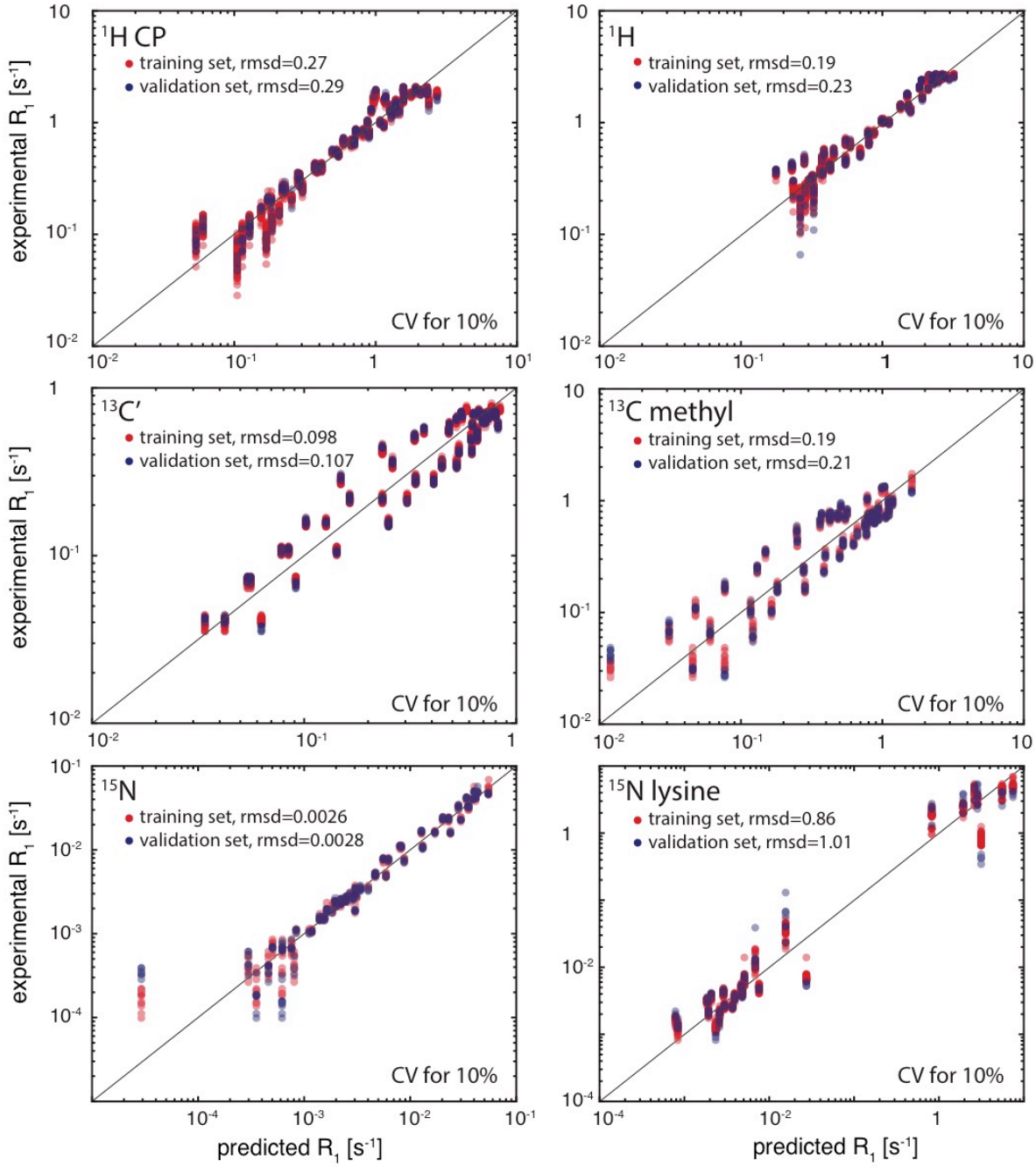

*Figure S6: Scatterplots showing the experimental against the predicted R_1 values for all the used probes. The predicted R_1 values are calculated using a model fit to 90% of the combined data sets (**I**, **II** and **III**). The red points show the training set and the blue points show the validation set. The black line corresponds to a one-to-one mapping between the experimental and predicted values.*

MD simulation

As described previously,[11] a "superlattice" of 32 copies of protein GB1 (equivalent to 8 unit cells of 4 proteins each), 4227 water molecules and 128 Na+ ions was constructed according to the crystallographic symmetry. The dimensions of the superlattice allow for a periodic box. Simulations were carried out using GROMACS 5.1.2[12] with the AMBER99SB force field.[13] After minimization using the steepest descent algorithm three independent 200 nanosecond trajectories were calculated at each of the four temperatures - 248, 258, 268 and 278 K. Angular correlation functions representing the motion of the relaxation-active interactions were analyzed as previously described, in terms of amplitudes and timescales of distinct motional modes:

$$C(t) = A_0 + \sum_{k=1}^{n} A_k e^{-t/\tau_k}$$

with n=3 for all cases discussed here. Most notably the amplitude of motions derived from the fit of the correlation functions are seen to vary with respect to temperature, but within a very restricted way (figure 5 in main manuscript).

The characterization of the effective timescales extracted from these fits is less easy to compare with experiment, firstly because characteristic timescales are less accurately predicted from MD simulation than motional amplitudes (see Figure S5 below) and secondly because the number of relaxation active contributions at higher temperatures are not equivalent to the experimental study (where one main contribution is assumed to contribute). Nevertheless, the trends seen to qualitatively reproduce experimental observation.

As an example, correlation functions from amino acids in each of the 32 copies of the protein in the simulation box were averaged and fitted to a three-exponential fit (figure S6). Note, that most of the temperature-dependent variation of the curve is due to the amplitude of very fast motions (i.e. the value of the correlation function at its first plotted point, 10 ps) Average timescales derived from the weighted averaged of the results of the fit show systematic changes in timescale (from 0.76 to 1.3 ns over the range of 278 to 248 K). This would correspond to an effective activation energy of 12 $kJmol^{-1}$ (figure S5B).

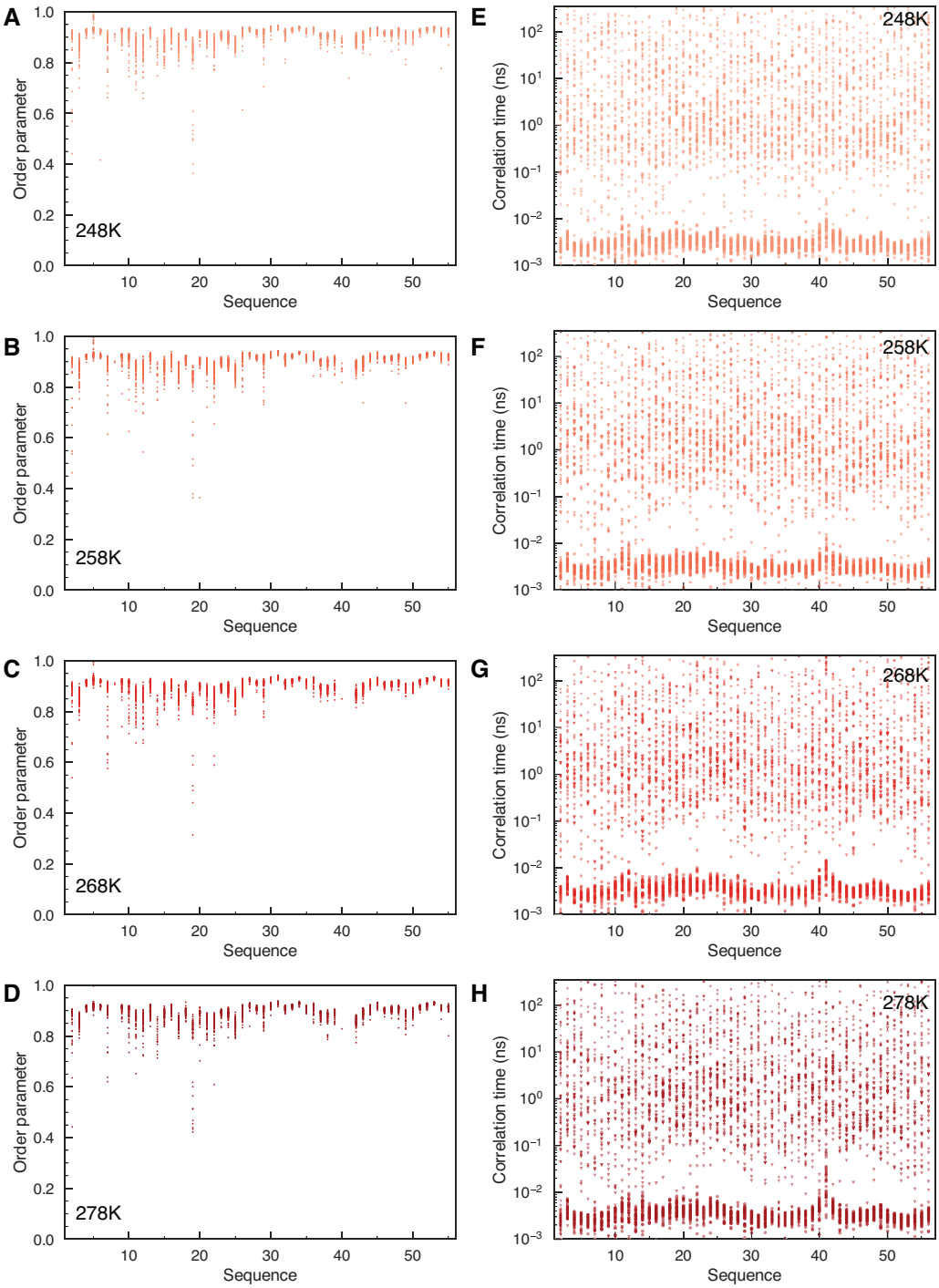

Figure S7: Order parameters calculated for each of the 32 copies of the protein in the superlattice at 248 (panel A), 258 (B), 268 (C) and 278 K (D) are clustered around a well-defined average value, providing a useful comparison with experimentally-determined parameters. On the contrary, motional timescales (panels E-H), with the exception of the fast component around 5 ps, are much more scattered, thereby hindering any quantitative comparison with the experimental results.

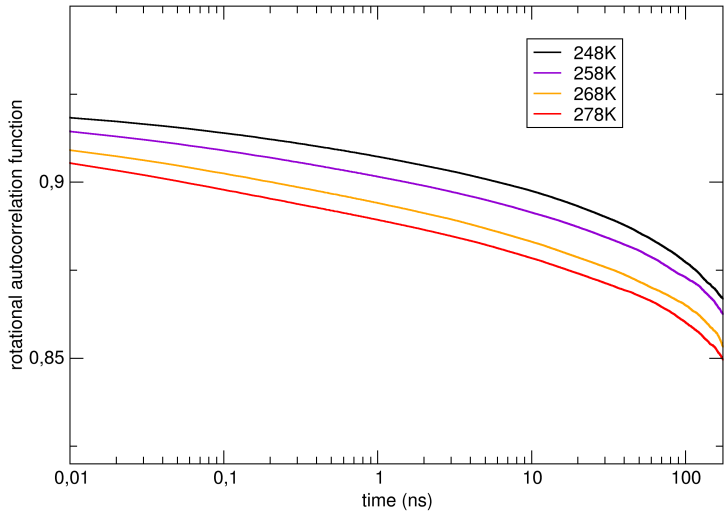

Figure S8: Average rotational correlation function of backbone NH bonds calculated as described above. Note the most evident differences between the curves for different temperatures results from the increasing amplitude of the fast (<10 ps) initial decay of the correlation function.

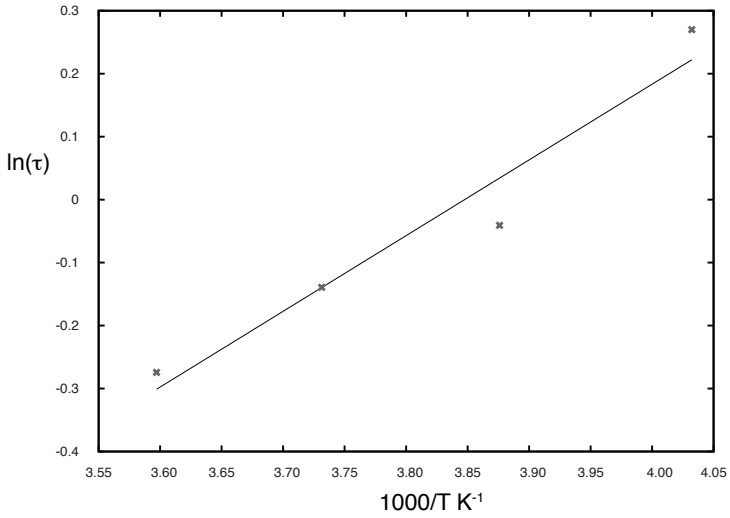

Figure S9: Timescales resulting from the fit of individual correlation functions (see Figure S6) at each temperature – points show averages over 32 copies of 56 N-H pairs. Calculated values (points) are fit to an Arrhenius relationship with effective activation energy of 12kJmol-1 (line). Averages are weighted by their contribution to the associated correlation function.

71. Franks, W. T.; Zhou, D. H.; Wylie, B. J.; Money, B. G.; Graesser, D. T.; Frericks, H. L.; Sahota, G.; Rienstra, C. M., Magic-angle spinning solid-state NMR spectroscopy of the beta1 immunoglobulin binding domain of protein G (GB1): 15N and 13C chemical shift assignments and conformational analysis. *J. Am. Chem. Soc.* **2005,** *127*, 12291-12305.

2. Bockmann, A.; Gardiennet, C.; Verel, R.; Hunkeler, A.; Loquet, A.; Pintacuda, G.; Emsley, L.; Meier, B. H.; Lesage, A., Characterization of different water pools in solid-state NMR protein samples. *J. Biomol. Nmr.* **2009,** *45*, 319-327.

3. Tycko, R., NMR at low and ultralow temperatures. *Acc. Chem. Res.* **2013,** *46*, 1923-1932.

4. Jacso, T.; Franks, W. T.; Rose, H.; Fink, U.; Broecker, J.; Keller, S.; Oschkinat, H.; Reif, B., Characterization of membrane proteins in isolated native cellular membranes by dynamic nuclear polarization solid-state NMR spectroscopy without purification and reconstitution. *Angew. Chem., Int. Ed.* **2012,** *51*, 432-435.

5. Ni, Q. Z.; Markhasin, E.; Can, T. V.; Corzilius, B.; Tan, K. O.; Barnes, A. B.; Daviso, E.; Su, Y.; Herzfeld, J.; Griffin, R. G., Peptide and protein dynamics and low-temperature/DNP magic angle spinning NMR. *J. Phys. Chem. B* **2017,** *121*, 4997-5006.

6. Debelouchina, G. T.; Bayro, M. J.; Fitzpatrick, A. W.; Ladizhansky, V.; Colvin, M. T.; Caporini, M. A.; Jaroniec, C. P.; Bajaj, V. S.; Rosay, M.; Macphee, C. E.; Vendruscolo, M.; Maas, W. E.; Dobson, C. M.; Griffin, R. G., Higher order amyloid fibril structure by MAS NMR and DNP spectroscopy. *J. Am. Chem. Soc.* **2013,** *135*, 19237-19247.
7. Lamley, J. M.; Lewandowski, J. R., Relaxation-based magic-angle spinning NMR approaches for studying protein dynamics. *eMagRes* **2016,** *5*, 1423-1433.
8. Redfield, A. G., Relaxation theory: Density matrix formulation. In *Encyclopedia of Magnetic Resonance*, John Wiley & Sons, Ltd: 2007.
9. Beckmann, P. A.; Buser, C. A.; Mallory, C. W.; Mallory, F. B.; Mosher, J., Methyl reorientation in solid 3-ethylchrysene and 3-isopropylchrysene. *Solid State Nucl. Magn. Reson.* **1998,** *12*, 251-256.
10. Lewandowski, J. R.; Halse, M. E.; Blackledge, M.; Emsley, L., Direct observation of hierarchical protein dynamics. *Science* **2015,** *348*, 578-581.
11. Mollica, L.; Baias, M.; Lewandowski, J. R.; Wylie, B. J.; Sperling, L. J.; Rienstra, C. M.; Emsley, L.; Blackledge, M., Atomic-resolution structural dynamics in crystalline proteins from NMR and molecular simulation. *J. Phys. Chem. Lett.* **2012,** *3*, 3657-3662.
12. Abraham, M. J.; Murtola, T.; Schulz, R.; Páll, S.; Smith, J. C.; Hess, B.; Lindahl, E., GROMACS: High performance molecular simulations through multi-level parallelism from laptops to supercomputers. *SoftwareX* **2015,** *1-2*, 19-25.
13. Hornak, V.; Abel, R.; Okur, A.; Strockbine, B.; Roitberg, A.; Simmerling, C., Comparison of multiple Amber force fields and development of improved protein backbone parameters. *Proteins* **2006,** *65*, 712-725.